Silicon (2020) 12:1213–1223
https://doi.org/10.1007/s12633-019-00223-4

ORIGINAL PAPER

Lanthanide-Doping Effects on the Formation of Leucite $KAlSi_2O_6$

A. Sabaliauskiene[1] · A. Beganskiene[1] · K. Ishikawa[2] · A. Kareiva[1]

Received: 11 April 2019 / Accepted: 3 July 2019 / Published online: 15 July 2019

Abstract

In this study, the lanthanide-doping (Ce^{3+}, Sm^{3+}, Eu^{3+} and Tb^{3+}) effects on the formation of leucite ($KAlSi_2O_6$) by sol-gel synthesis were investigated. The phase purity and morphological properties of lanthanide-doped specimens have been estimated. The proposed sol-gel synthesis route is suitable for the preparation of mixed leucite-kalsilite ceramics doped with Sm^{3+}, Eu^{3+} and Tb^{3+} (up to 10 M %). This simple and successful synthetic approach offers a feasible way to obtain lanthanide-doped potassium alumosilicate ceramics with possible application in odontology. The synthesis products were characterized using thermal analysis (TG/DTA), X-ray powder diffraction (XRD) analysis, infrared spectroscopy (FTIR) and scanning electron microscopy (SEM). Moreover, the optical properties of lanthanide-doped synthesis products were also investigated.

Keywords Silicate ceramic · Functional materials · Biomedical applications · Sol-gel processes · Optical properties

1 Introduction

The development of new materials or new synthesis routes for novel materials applicable in medicine still presents numerous challenges [1, 2]. The ceramics, glasses, bulk materials and thin/thick films are used in biotechnology and biomedicine for many years, however, the search a novel biomaterials to substitute hard tissues and, consequently, to reach better quality of life is the principle task for the scientists working in this area. The huge number of different biomaterials is widely used in orthopedics and odontology [3–8]. Current applications include total and partial replacements of hip, knee, teeth, and different bone reconstructions after surgeries [9].

Highlights
- The lanthanide-doped leucite samples were synthesized using sol-gel synthesis route.
- Leucite-kalsilite ceramics doped with Sm^{3+}, Eu^{3+} and Tb^{3+} were obtained.
- Contraray, the single-phase undoped leucite ceramic was obtained at 1000 °C.
- Luminescent properties of lanthanide-doped ceramics were investigated.
- Lanthanide-doped potassium alumosilicate ceramics could be applied in odontology.

✉ A. Kareiva
aivaras.kareiva@chgf.vu.lt

[1] Institute of Chemistry, Vilnius University, Naugarduko 24, LT-03225 Vilnius, Lithuania

[2] Department of Biomaterials, Faculty of Dental Science, Kyushu University, Maidashi, Higashi-Ku, Fukuoka, Japan

Silica based bioceramics are probably the largest group of biomaterials. The system of SiO_2-Na_2O-CaO-P_2O_5 with additions of B_2O_3 and CaF_2 was first demonstrated forming a strong bond with bone [10]. The porcelain fused to metal (PFM) crowns were started to use already many years ago. Alkali-modified alumosilicate glasses became the predominant matrix material for dental restorations [11, 12]. The dental porcelains for metal–ceramic systems contain leucite (K_2O-Al_2O_3-$4SiO_2$ or $KAlSi_2O_6$) as the main crystalline phase to increase the thermal expansion coefficient (CTE) and the mechanical resistance of the porcelain [13, 14]. It was demonstrated, that the understanding of the interconnectivity between fatigue, wear and secondary caries formation is essential key for the successful development of improved dental restorative materials. Moreover, the dental porcelains containing leucite are able to ensure required translucency similar to the natural tooth [14–18]. Summarizing the results presented in these articles it is clear, that to maximize aesthetics and durability of dental ceramics remain the most important problems. Additional oxides could serve the formation of desired colour of porcelains to avoid the darkness of metallic frameworks, since the dental ceramic is fused to various metal alloys. The combination of two different crystal phases including leucite and fluorapatite for the dental ceramics was also suggested by several authors [19–24].

Natural leucite crystallizes at high temperature in a cubic form, however, below 665 °C it transforms to tetragonal phase [25, 26]. The leucite powders were synthesized by co-precipitation, hydrothermal and solid state reaction methods. The synthesis of leucite by hydrothermal method was reported elsewhere [27–31]. The crystallization of leucite using solid-

state reactions is reported in [32–36]. The precursor for the preparation of $KAlSi_2O_6$ was synthesized also by sol–gel method when KNO_3, $Al(NO_3)_3{\cdot}12H_2O$ and TEOS were used as raw materials [37]. However, the synthesis of monophasic leucite at relative low temperature is very problematic [38–41]. The synthesis products additionally contained amorphous and kalsilite phases [38, 40] or unreacted starting materials along with kalsilite [39, 41].

Glasses and silicate materials are promising host materials to investigate the influence of chemical environment on the optical properties of the rare earth ions [42–46]. The alkaline earth alumosilicates possess wide band gap energies at about 5.0 eV. It makes them as suitable host materials to study specific interactions in dopant rare-earth ions [47–50]. Several researchers have noted that co-doping with Al^{3+} is effective for the dispersing of rare earth ions in silicate matrices [51–54].

Previously, we developed an efficient and environmentally friendly aqueous sol-gel synthesis method for the preparation of monophasic leucite [55]. In this study, the formation peculiarities and properties of lanthanide-doped (Ce^{3+}, Eu^{3+}, Sm^{3+} and Tb^{3+}) K_2O-Al_2O_3-$4SiO_2$ ceramics are discussed.

2 Experimental

2.1 Materials

For the sol-gel preparation of lanthanide-doped and undoped leucite, aluminium nitrate nonahydrate $Al(NO_3)_3.9H_2O$ (≥98% Aldrich), silica dioxide SiO_2 (fumed, >99% Merck), samarium oxide Sm_2O_3 (99.9% Alfa Aesar), europium oxide Eu_2O_3 (99.9% Alfa Aesar), terbium oxide Tb_4O_7 (99,9% Alfa Aesar), ammonium cerium nitrate $(NH_4)_2Ce(NO_3)_6$ (≥99% Fluka), potassium hydroxide KOH (90% Aldrich), nitric acid HNO_3 (67% Reachem) and 1,2-ethanediol $C_2H_6O_2$ (EG) (99,0% Alfa Aesar) were used as starting materials.

2.2 Synthesis

To study lanthanide substitution effects on the formation of leucite, the Eu, Ce, Tb and Sm ions were selected as dopants in the leucite matrix. The samples with different amounts of dopants were prepared by previously developed sol-gel synthesis method. In the sol-gel processing, the fumed silicon dioxide was dispersed in small amount (~ 50 ml) of distilled water and mixed with the potassium hydroxide dissolved in 25 ml of distilled water with 1, 2–ethanediol as complexing agent. After few hours of stirring the opaque solution has formed. The rear earth metal oxides were dissolved in nitric acid to form soluble nitrates and mixed with 1, 2–ethanediol and added to the above solution. After 1 h, the aluminium nitrate dissolved in water with 1, 2–ethanediol was slowly added to the solution. The 1,2-etahendiol was added in all steps to ensure the homogeneity of the final sol. The sol was then turned to the gel by slow evaporation of solution at ~ 70 °C and then dried for 24 h at 100 °C. The dried gels were heated at 500 °C for 5 h with a heating rate of 1 °C/min to

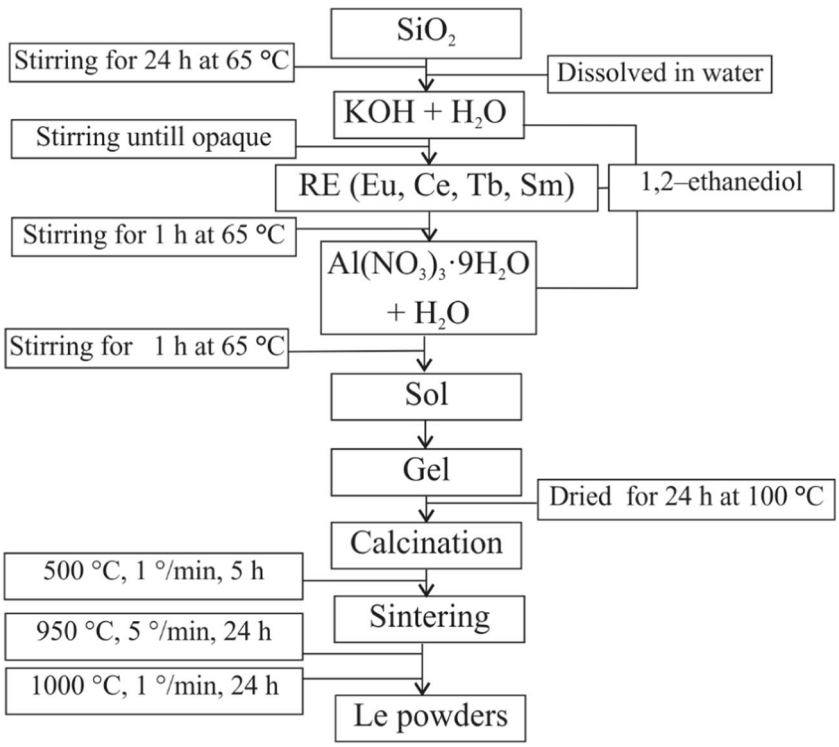

Fig. 1 A schematic diagram of sol-gel processing of lanthanide-doped leucite

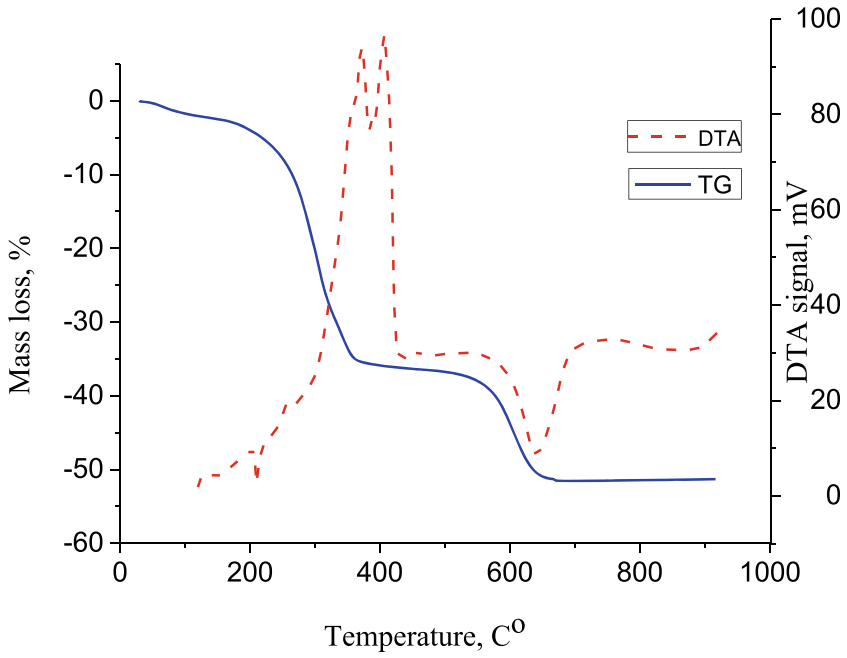

Fig. 2 TG/DTA curves of samarium-doped K-Al-Si-O gel precursors

remove organic and nitrate components. The obtained powders were heated at 900 °C and at 1000 °C for 24 h with a heating rate of 5 °C/min. The ceramic samples were named using following labels leucite:Eu – E-005, E-01, E-02, E-05, E-10, leucite:Ce – Ce-005, Ce-01, Ce-02, Ce-05, Ce-10, leucite:Tb – Tb- 005, Tb-01, Tb-02, Tb-05, Tb-10 and leucite:Sm – Sm-005, Sm-01, Sm-02, Sm-05, Sm-10. The number indicates rear earth ion concentration, e. g. Sm-10 indicates that samarium concentration is 10 mol% in the leucite matrix. The scheme of the sol-gel preparation of lanthanide-doped leucite samples is presented in Fig. 1. For the comparison, the synthesis of undoped leucite using the same procedure was also performed.

2.3 Characterization

Thermogravimetry/differential thermal analysis (TG/DTA) of the Ln:K-Al-Si-O (here Ln – is lanthanide element) precursor gels was carried out in air at a heating rate of 10 °C/min using Simultaneous Thermal analyser STA6000

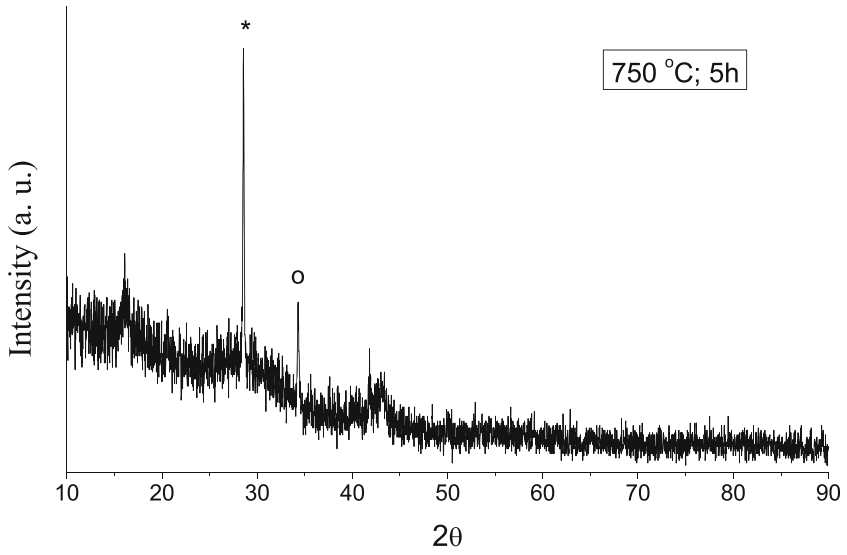

Fig. 3 XRD patterns of Eu:K-Al-Si-O gel precursors annealed at 750 °C for 5 h. The main crystalline phases are marked: * - SiO_2 and o – $Al_2O_3{\cdot}2SiO_2{\cdot}2H_2O$

from PerkinElmer. Powder X-ray diffraction analysis (XRD) was performed with Rigaku MiniFlex II (with the Bragg-Brentano (θ/2θ) geometry) diffractometer. The data was collected using CuK_α radiation. The functional groups in the samples were characterized by FTIR spectroscopy using Perkin-Elmer FTIR Spectrum BX II spectrometer. The morphology of the resulting products was determined with a field emission scanning electron microscope FE-SEM, Hitachi SU-70. The photoluminescence excitation and emission spectra were measured with PerkinElmer (LS 55 Fluorescence) spectrometer.

3 Results and Discussion

For the investigation of lanthanide substitution effects in leucite four lanthanide elements Ce^{3+}, Sm^{3+}, Eu^{3+} and Tb^{3+} were selected. The series of $KAlSi_2O_6:Ln_x$ (x = 0.005; 0.01; 0.02; 0.05 and 0.1 or 0.5; 1.0; 2.0; 5.0 and 10.0 mol%, respectively) were synthesized using an aqueous sol-gel method. The thermal decomposition of the lanthanide-doped K-Al-Si-O gel precursors was studied from room temperature up to 950 °C. TG/DTA curves of the representative samarium-doped K-Al-Si-O gel are shown in Fig. 2. As seen, three important mass losses could be determined in the TG curve. The first step of mass loss (about 4%) up to 150 °C is associated to the evolution of adsorbed moisture [56]. This is in a good agreement with visible endotherm in the DTA curve. The second and the main mass loss of about 35% is observed in the temperature range of 150–380 °C and can be attributed to the thermal decomposition of organic part of the gel. Evidently, this mass loss step is accompanied by two very intensive exothermic signals in DTA curve. The last mass loss of about 14% is observed in the temperature range of 575–650 °C due to the final decomposition of formed carbonate and possible crystallization of potassium alumosilicate. The endothermic peak apparently proves this assumption. No more mass losses could be observed above 650 °C. The total mass loss was about 53%. Thermal decomposition behaviour of other lanthanide-doped K-Al-Si-O gels was almost identical.

Taking into account the obtained TG results (full decomposition at 650 °C), the initial synthesis of leucite was performed at slightly higher temperature (700 °C). The representative XRD pattern of europium-doped synthesis product is demonstrated in Fig. 3. The XRD

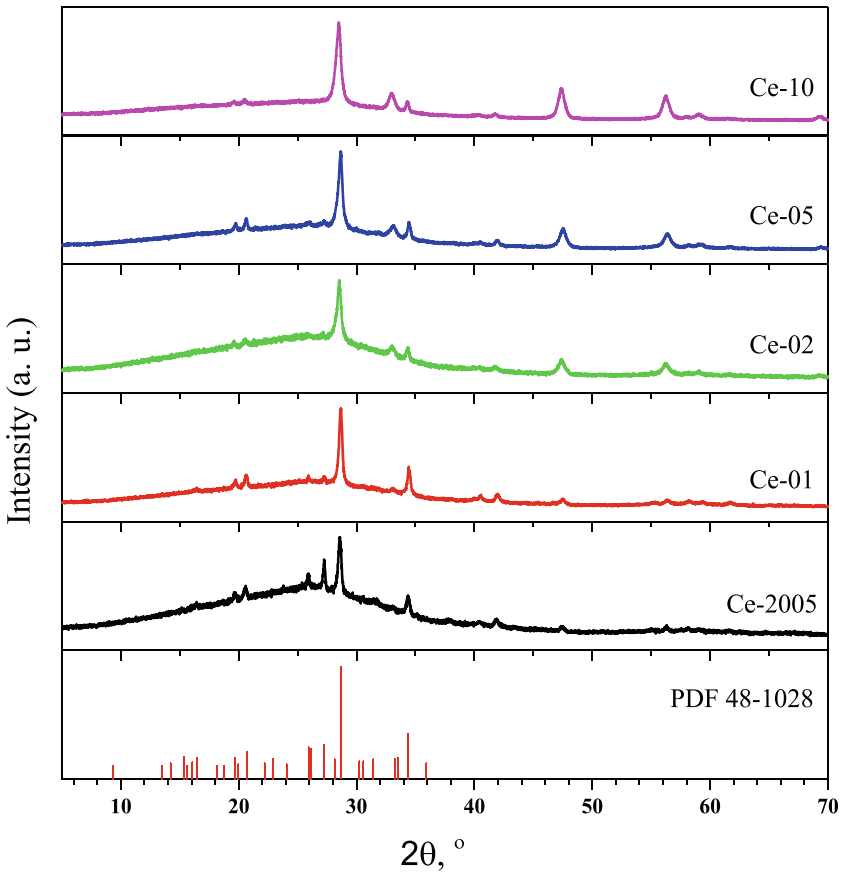

Fig. 4 XRD patterns of alumosilicate samples doped with different amount of Ce^{3+} and annealed at 1000 °C. Vertical lines represent standard XRD pattern of kalsilite

results showed that after heating of Ln:K-Al-Si-O gel precursors at 700 °C for 5 h partially amorphous materials were obtained. The separate crystalline phases of silica and kaolinite could be detected from the XRD pattern. Thus, further annealing of lanthanide-doped K-Al-Si-O precursor gels was performed at higher temperatures. XRD patterns of the reaction products doped with different amount of Ce^{3+}, Eu^{3+}, Sm^{3+} and Tb^{3+} ions and obtained at 1000 °C for 24 h are shown in Figs. 4, 5, 6 and 7, respectively. The XRD patterns of samples doped with Ce, however, mostly consist of diffraction lines attributable to the kalsilite ($KAlSiO_4$) phase with no diffraction peaks of leucite (see Fig. 4). The successful cerium doping only in bioactive glasses was previously reported [57, 58]. Figure 5 shows the XRD patterns of europium doped leucite samples. As seen from XRD pattern at low concentration of europium (0.5 mol%) the synthesis product is composed of two crystalline phases of leucite and kalsilite. By increasing concentration of europium to 1 mol% the leucite phase becomes predominant and only traces of kalsilite could be identified. However, with further increasing concentration of Eu^{3+} to 10 mol% the mixture of kalsilite and leucite phases has formed. Very similar XRD results were obtained for the samples doped with Sm and Tb (see Figs. 6 and 7, respectively). As seen, the leucite crystallizes along with kalsilite phase in both cases. In both cases the XRD patterns with dopant concentration of 0.5 mol% contain low intensity of leucite and kalsilite peaks. By increasing concentration to 1 mol% the mixture of kalsilite and leucite phases could be easily identified. With increasing of Sm^{3+} and Tb^{3+} to 2.0 mol% the intensity of diffraction peaks decreases, whereas further addition of dopants to 5 and 10 mol% increased the intensity of peaks. This could be due to the intermediate role of dopant in the formation of ceramic structure.

The obtained results inspired us to repeat the same sol-gel synthesis of undoped leucite at slightly different temperatures. The XRD patterns of the K-Al-Si-O gel sample heated at 950 and 1000 °C are presented in Fig. 8. The results clearly show that almost monophasic leucite has formed at 950 °C and single-phase high crystalline leucite was obtained at 1000 °C. Thus, the question why lanthanide elements resist the formation of pure leucite and promote at the same time the partial formation of kalsilite still remains open. Due to the lack of literature data the reason of formation of the mixture

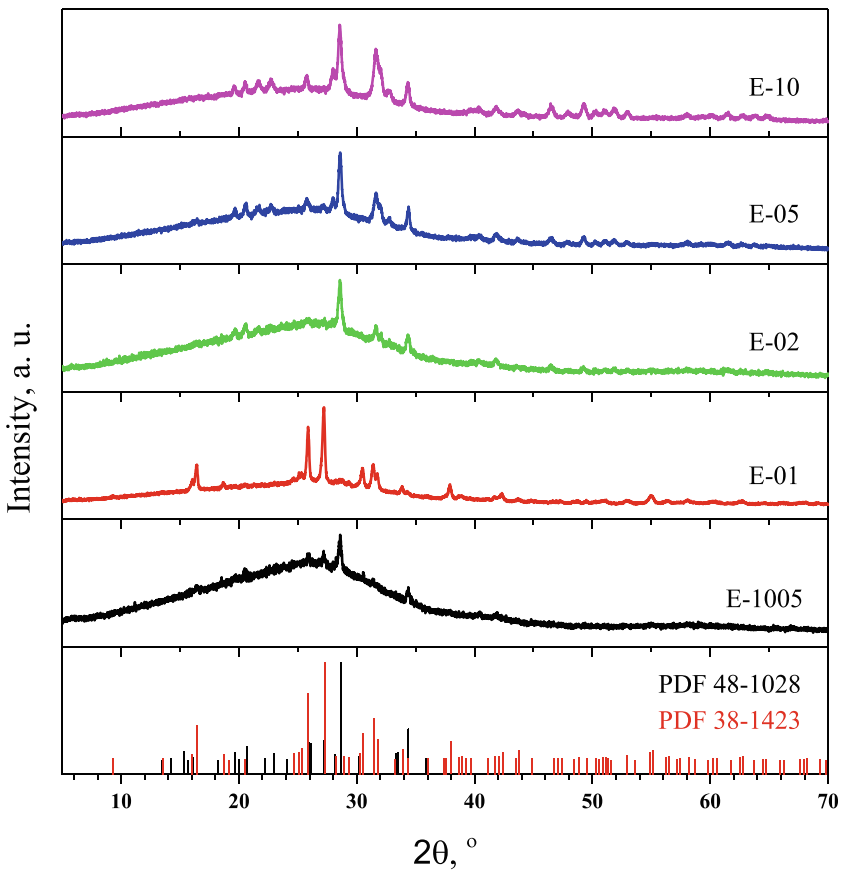

Fig. 5 XRD patterns of alumosilicate samples doped with different amount of Eu^{3+} and annealed at 1000 °C. Vertical lines represent standard XRD patterns of leucite and kalsilite

of kalsilite and leucite phases induced by lanthanide doping remains unclear.

The FTIR spectra of lanthanide-doped alumosilicate samples are given in Fig. 9. It is obvious that all FTIR spectra are very similar independent on the nature of dopant element. The broad bands observed at 3500–3330 cm^{-1} and weak bands at 1620–1640 cm^{-1} correspond to O-H stretching vibrations originated from adsorbed moisture from atmosphere [59]. The Si-O-Si stretching vibrations are located at around 1000–970 cm^{-1}, and the Si-O-(Si, Al) stretching vibrations are in the range of 670–580 cm^{-1} [37, 60, 61]. Nevertheless, the negligible shift of the Si-O and Al-O vibration bands by introducing the lanthanide element has been observed [55]. On the other hand, all FTIR spectra are almost identical independently on the used lanthanide element as dopant. The FTIR results are in a good agreement with XRD data.

The surface morphology of all lanthanide-doped alumosilicate samples was analysed by SEM. Since all samples possessed very similar surface morphology, only representative SEM micrograph of Eu-doped sample is presented in Fig. 10. The formation of irregular plate-like shaped particles is determined for the sol-gel derived lanthanide-doped alumosilicate ceramics. The size of particles varies from 0.5 to 25 μm. According to SEM images, the interconnected pores are also formed in the synthesized alumosilicates [62].

Figure 11 shows emission and excitation spectra of Eu^{3+}-doped (5 mol%) leucite-kalsilite sample. All europium containing samples exhibited a maximum excitation peak at ~394 nm along with 364, 374, 381, 414 and 464 nm. The broad and intensive band ranging from 250 to 350 nm is attributed to the charge transfer (CT) transition which can be written as $Eu^{3+} + O^{2-} \leftrightarrow Eu^{2+} + O^{-}$ [63, 64]. Emission spectrum was obtained upon excitation at 265 nm. The luminescence spectrum consists of broad lines associated with $^5D_0 \rightarrow {}^7F_{0-4}$ transition (570–710 nm, orange-red region) of Eu^{3+} ions with the hypersensitive line at 616 nm [63, 64]. The excitation and emission spectra of Tb^{3+}-doped bioceramic are shown in Fig. 12. The range from 200 to 310 nm comprises of $[Xe]4f^8 \rightarrow [Xe]4f^75d^1$ very intensive transitions [65]. The range from 310 to 500 nm represents $[Xe]4f^8 \rightarrow [Xe]4f^8$ transitions [65]. Emission spectra were obtained upon excitation at 260 nm. The spectra indicate typical emission lines of Tb^{3+} ions at around 419, 440, 460, 487, 547, 550, 586 and 623 nm [65, 66]. The emission peak at 547 nm is dominant. Interestingly, the potassium alumosilicate samples doped with cerium and samarium did not exhibit the photoluminescence properties. For

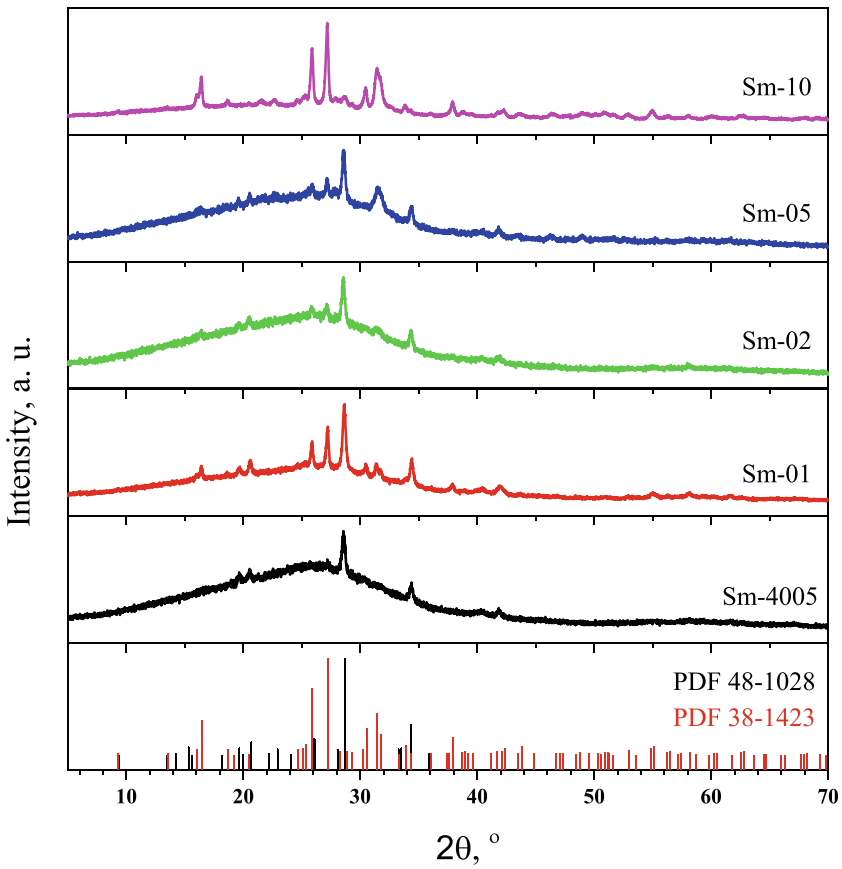

Fig. 6 XRD patterns of alumosilicate samples doped with different amount of Sm^{3+} and annealed at 1000 °C. Vertical lines represent standard XRD patterns of leucite and kalsilite

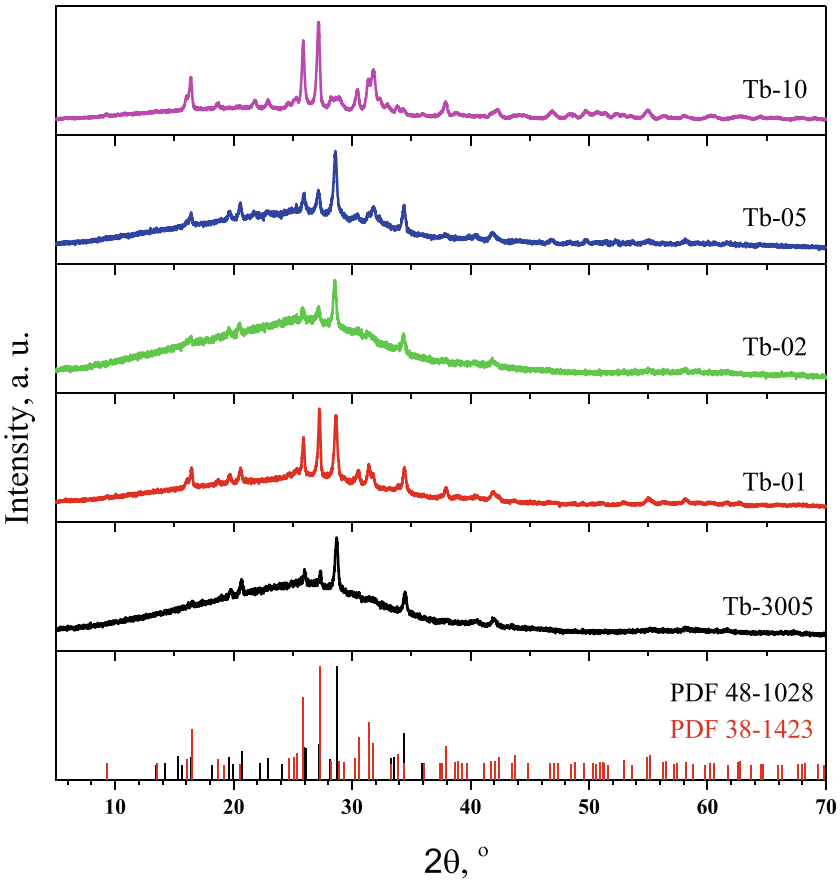

Fig. 7 XRD patterns of alumosilicate samples doped with different amount of Tb^{3+} and annealed at 1000 °C. Vertical lines represent standard XRD patterns of leucite and kalsilite

example, the reason for the lower photoluminescent activity of cerium-doped samples was attributed to a great Ti^{3+}/Ti^{4+} ratio and a large amount of hydroxyl oxygen found in pure TiO_2 [67]. It was also demonstrated that the Ce single doped silica samples exhibited very poor emission [68]. The co-doping is using to promote the luminescence of Sm^{3+} indicating that energy could be transferred from other lanthanides to Sm^{3+} [69, 70].

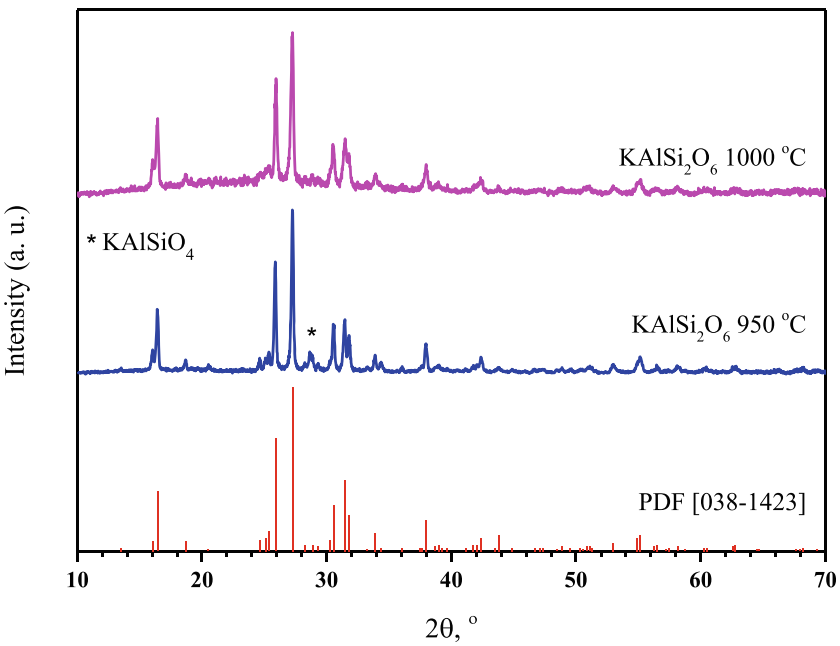

Fig. 8 XRD patterns of leucite obtained at different temperatures. Vertical lines represent standard XRD pattern of leucite

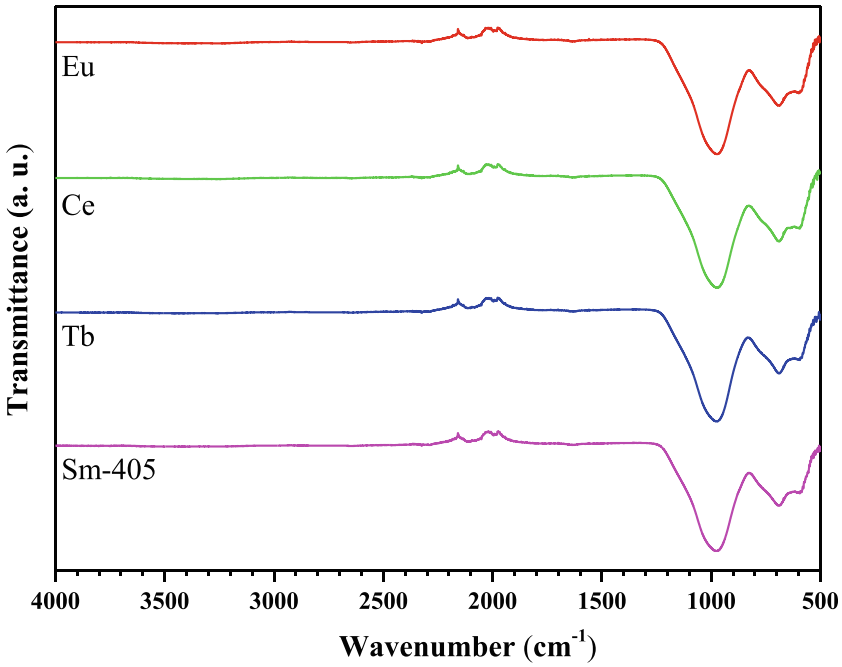

Fig. 9 FTIR spectra of lanthanide-doped (5 mol%) alumosilicate (mixture of leucite and kalsilite) samples

4 Conclusions

The sol-gel synthesis method was applied for the preparation of lanthanide-doped (Ce^{3+}, Sm^{3+}, Eu^{3+} and Tb^{3+}) leucite ($KAlSi_2O_6$) samples. The Ce^{3+} doped samples, however, inhibited leucite formation favouring the crystallization of kalsilite ($KAlSiO_4$). Contrary, during the sol-gel synthesis of Eu^{3+}-, Tb^{3+}- and Sm^{3+}- doped leucite samples the mixtures of both leucite and kalsilite phases have formed. Interestingly, the single-phase undoped leucite ceramic was obtained at 1000 °C using the same aqueous sol-gel synthesis route. According to the SEM measurements, all synthesized samples possessed very similar surface morphology. Luminescent

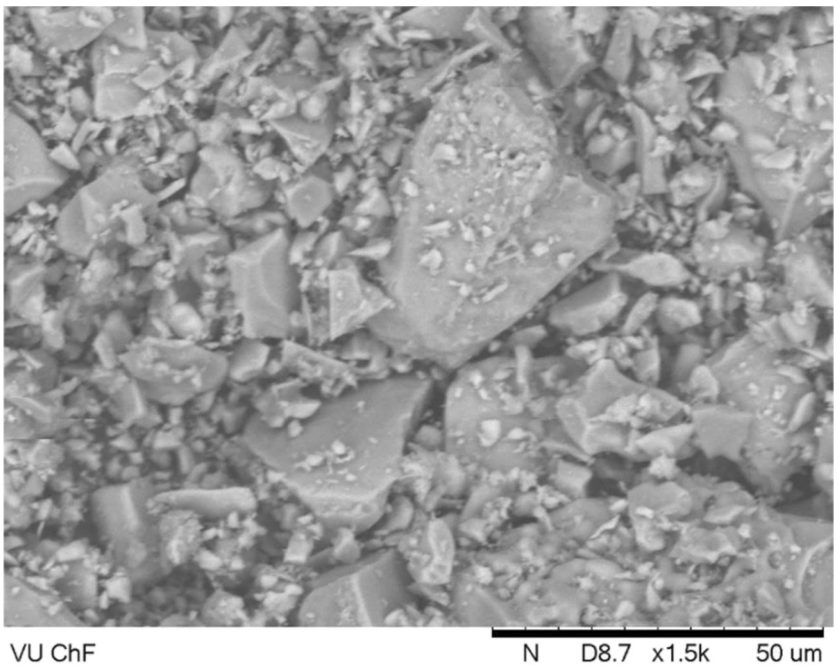

Fig. 10 SEM micrograph of Eu-doped (2.5 mol%) alumosilicate sample

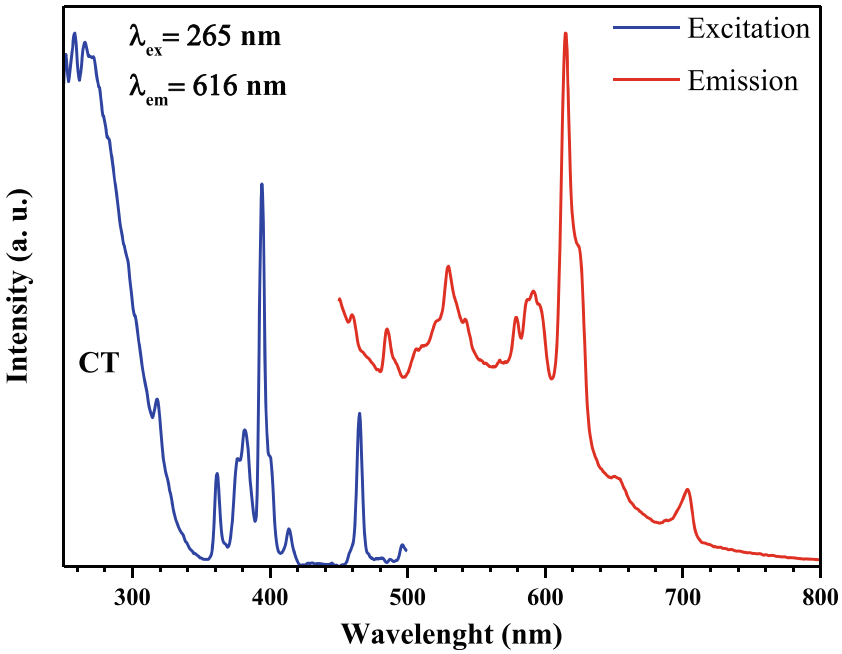

Fig. 11 Excitation and emission spectra of Eu^{3+}-doped (5 mol%) potassium alumosilicates sample

properties of lanthanide - doped leucite-kalsilite samples were also investigated. Emission spectrum of Eu^{3+}-doped (5 mol%) sample was obtained upon excitation at 265 nm and consisted of broad lines associated with $^5D_0 \rightarrow {}^7F_{0-4}$ transition (570–710 nm, orange-red region) of Eu^{3+} ions with the most intensive line at 616 nm. The luminescence spectrum of Tb^{3+}-doped ceramic upon excitation at 260 nm showed the dominant emission peak at 547 nm. The Eu^{3+} and Tb^{3+} containing alumosilicate samples showed luminescence under UV radiation, however, the similarly obtained Ce^{3+}- and Sm^{3+}-doped samples did not exhibit any photol uminescence properties. The Eu^{3+} and Tb^{3+} containing alumosilicate samples could be used for the formation of desired colour and shade of dental porcelains for the aesthetics purposes.

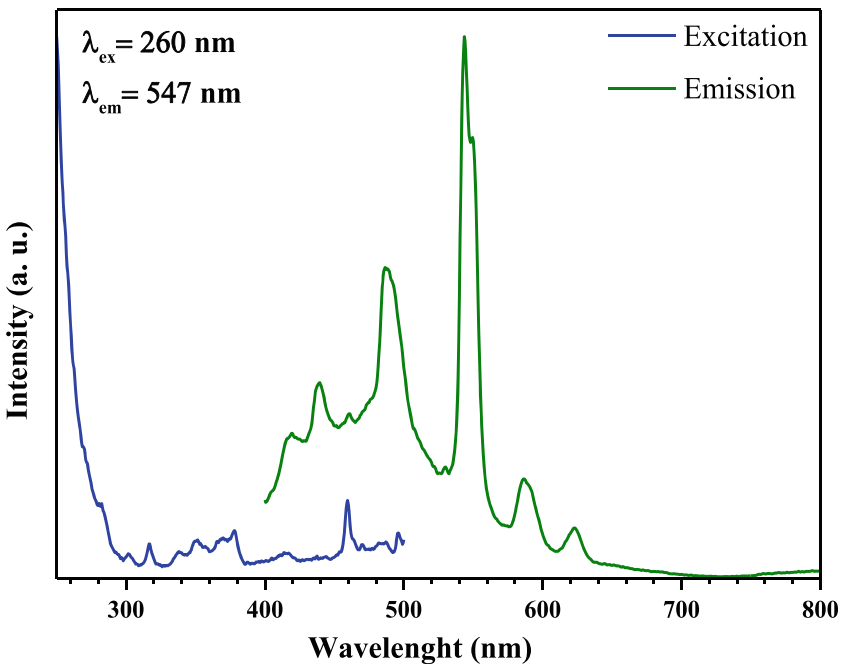

Fig. 12 Excitation and emission spectra of Tb^{3+}-doped (5 mol%) potassium alumosilicates sample

Acknowledgments AK would like to express sincere gratitude for Fellowship administrated by The Japan Society for the Promotion of Science (JSPS). Fellow's ID No.: L12546.

Compliance with Ethical Standards

Conflict of Interest The authors declare that they have no conflict of interest.

References

1. Kaur S, Bala N, Khosla C (2019) Investigations of thermal sprayed HAP and HAP-TiO_2 composite coatings for biomedical applications. Anti-Corros Methods Mater 66:74–87
2. Abumanhal M, Ben-Cnaan R, Feldman I, Keren S, Leibovitch I (2019) Polyester urethane implants for orbital trapdoor fracture repair in children. J Oral Maxillofac Surg 77:126–131
3. Best SM, Porter AE, Thian ES, Huang J (2008) Bioceramics: past, present and for the future. J Eur Ceram Soc 28:1319–1327
4. Avnir D, Coradin T, Lev O, Livage J (2006) Recent bio-applications of sol-gel materials. J Mater Chem 16:1013–1030
5. Cabal B, Malpartida F, Torrecillas R, Hoppe A, Boccaccini AR, Moya JS (2011) The development of bioactive glass-ceramic substrates with biocide activity. Adv Eng Mater 13:B462–B466
6. Gao A, Hang RQ, Huang XB, Zhao LZ, Zhang XY, Wang L, Tang B, Ma SL, Chu PK (2014) The effects of titania nanotubes with embedded silver oxide nanoparticles on bacteria and osteoblasts. Biomater 35:4223–4235
7. Shah FA, Thomsen P, Palmquist A (2018) A review of the impact of implant biomaterials on osteocytes. J Dent Res 97:977–986
8. Jia ZJ, Zhou WH, Yan JL, Xiong P, Guo H, Cheng Y, Zheng YF (2019) Constructing multilayer silk protein/nanosilver biofunctionalized hierarchically structured 3D printed Ti6Al4 V scaffold for repair of infective bone defects. ACS Biomater Sci Eng 5:244–261
9. Vallet-Regi M (2001) Ceramics for medical applications. J Chem Soc Dalton Trans:97–108
10. Hench LL, Paschall HA (1973) Direct chemical bond of bioactive glass-ceramic materials to bone and muscle. J Biomed Mater Res 7: 25–42
11. Kelly JR (1997) Ceramics in restorative and prosthetic dentistry. Annu Rev Mater Sci 27:443–468
12. Thomsen RM, Skibsted J, Yue YZ (2018) The charge-balancing role of calcium and alkali ions in per-alkaline aluminosilicate glasses. J Phys Chem B 122:3184–3195
13. Barreiro MM, Vicente EE (1993) Kinetics of isothermal phase-transformations in a dental porcelain. J Mater Sci Mater Med 4: 431–436
14. Kruzic JJ, Arsecularatne JA, Tanaka CB, Hoffman MJ, Cesar PF (2018) Recent advances in understanding the fatigue and wear behavior of dental composites and ceramics. J Mech Behav Biomed Mater 88:504–533
15. Souza JCM, Nascimento RM, Martinelli AE (2010) Characterization of dental metal-ceramic interfaces immersed in artificial saliva after substructural mechanical metallization with titanium. Surf Coat Technol 205:787–792
16. Assmann S, Ermrich M, Kunzmann K (2001) High-temperature X-ray diffraction analysis of a low-fusing dental ceramic. J Mater Sci 36:5403–5406
17. Li XX, Shaw LL (2007) Formation of leucite-free zone in laser densified dental porcelains. Mater Lett 61:3946–3950
18. Kelly JR, Benetti P (2011) Ceramic materials in dentistry: historical evolution and current practice. Aust Dent J 56:84–96
19. Holand W, Rheinberger V, Apel E, van't Hoen C (2007) Principles and phenomena of bioengineering with glass-ceramics for dental restoration. J Eur Ceram Soc 27:1521–1526
20. Kukiattrakoon B, Hengtrakool C, Kedjarune-Leggat U (2010) Degradability of fluorapatite-leucite ceramics in naturally acidic agents. Dent Mater J 29:502–511
21. Fredericci C, Yoshimura HN, Molisani AL, Pinto MM, Cesar PF (2011) Effect of temperature and heating rate on the sintering of leucite-based dental porcelains. Ceram Int 37:1073–1078
22. Goudouri OM, Kontonasaki E, Papadopoulou L, Kantiranis N, Lazaridis NK, Chrissafis K, Chatzistavrou X, Koidis P, Paraskevopoulos KM (2014) Towards the synthesis of an experimental bioactive dental ceramic. Part I: crystallinity characterization and bioactive behavior evaluation. Mater Chem Phys 145:125–134
23. Ritzberger C, Schweiger M, Holand W (2016) Principles of crystal phase formation in Ivoclar Vivadent glass-ceramics for dental restorations. J Non-Cryst Solids 432:137–142
24. Maggetti M, D'Albis A (2017) Phase and compositional analysis of a Sevres soft paste porcelain plate from 1781, with a review of early porcelain techniques. Eur J Mineral 29:347–367
25. Paukov IE, Belitsky IA, Fursenko BA (2002) Heat capacity and thermodynamic functions of leucite at low temperatures. Thermochim Acta 387:23–28
26. Palmer DC, Salje EKH (1990) Phase-transitions in leucite – dielectric properties and transition mechanism. Phys Chem Miner 17: 444–452
27. Zhang Y, Lv M, Rao PG, Shui AZ (2007) Quantitative XRD analysis of hydrothermally-derived leucite content in dental porcelain ceramics. J Ceram Soc Jpn 115:329–332
28. Kohoutkova M, Klouzkova A, Kostka P, Mrazova M (2008) Synthesis and characterization of an amorphous precursor for leucite dental ceramics. J Non-Cryst Solids 354:741–748
29. Klouzkova A, Mrazova M, Kohoutkova M (2007) Synthesis of partially stabilized leucite. J Phys Chem Solids 68:1207–1210
30. Klouzkova A, Mrazova M, Kohoutkova M, Klouzek J (2013) Leucite dental ceramics. Chem List 107:856–861
31. Farrukh MA, Naseem F, Imtiaz A, Khaleeq-ur-Rahman M, Martins TD, Zia KM (2016) Hydrothermal synthesis of leucite nanoparticles using anionic surfactant: structural evaluation and catalytic properties. Russ J Phys Chem A 90:1231–1237
32. Cattell MJ, Chadwick TC, Knowles JC, Clarke RL, Samarawickrama DYD (2006) The nucleation and crystallization of fine grained leucite glass-ceramics for dental applications. Dent Mater 22:925–933
33. Chen XH, Chadwick TC, Wilson RM, Hill RG, Cattell MJ (2011) Crystallization and flexural strength optimization of fine-grained leucite glass-ceramics for dentistry. Dent Mater 27:1153–1161
34. Chen X, Chadwick TC, Wilson RM, Hill R, Cattell MJ (2010) Crystallization of high-strength fine-sized leucite glass-ceramics. J Dent Res 89:1510–1516
35. Tosic MB, Dimitrijevic RZ, Mitrovic MM (2002) Crystallization of leucite as the main phase in glass doped with fluorine anions. J Mater Sci 37:2293–2303
36. Li J, Duan JX, Hou L, Lu ZY (2018) Effect of Cs content on $K_{1-x}Cs_xAlSi_2O_6$ ceramic solidification forms. J Nucl Mater 499:144–154
37. Bogdanoviciene I, Jankeviciute A, Pinkas J, Beganskiene A, Kareiva A (2008) Study of alumosilicate porcelains: sol-gel preparation, characterization and erosion evaluated by gravimetric method. Mater Res Bull 43:2998–3007
38. Zhang Y, Wu JQ, Rao PG, Lv M (2006) Low temperature synthesis of high purity leucite. Mater Lett 60:2819–2823
39. Hashimoto S, Sato F, Honda S, Awaji H, Fukuda K (2005) Fabrication and mechanical properties of sintered leucite body. J Ceram Soc Jpn 113:488–490

40. Zhang Y, Lv M, Chen DD, Wu JQ, Rao PG (2007) Leucite crystallization kinetics with kalsilite as a transition phase. Mater Lett 61: 2978–2981
41. Xie N, Bell JL, Krivenw WM (2010) Fabrication of structural leucite glass-ceramics from potassium-based geopolymer precursors. J Am Ceram Soc 93:2644–2649
42. Annapurna K, Dwivedi RN, Kumar A, Chaudhuri AK, Buddhudu S (2000) Temperature dependent luminescence characteristics of Sm^{3+}-doped silicate glass. Spectrochim Acta A Mol Biomol Spectrosc 56:103–109
43. Chimalawong P, Kaewkhao J, Kedkaew C, Limsuwan P (2010) Optical and electronic polarizability investigation of Nd^{3+}-doped soda-lime silicate glasses. J Phys Chem Solids 71:965–970
44. Eslami M, Hamnabard Z, Ali N (2013) Synthesis and spectral properties of Nd-doped glass-ceramics in SiO_2-CaO-MgO system prepared by sol-gel method. J Rare Earths 31:595–599
45. Rego FG, Dantas NO, Silva ACA, Vermelho MVD, Jacinto C, Gouveia-Neto AS (2017) IR-to-visible frequency upconversion in Yb^{3+}/Tm^{3+} co-doped phosphate glass. Opt Mater 73:1–6
46. Sobczyk M, Marek L (2019) Comparative study of optical properties of Ho^{3+} −doped RE_2O_3-Na_2O-ZnO-TeO_2 glasses. J Lumin 206: 308–318
47. Sontakke AD, Biswas K, Annapurna K (2009) Concentration-dependent luminescence of Tb^{3+} ions in high calcium aluminosilicate glasses. J Lumin 129:1347–1355
48. Sun T, Li R, Chen JJ, Mao ZY, Wang YZ, Wang DJ (2016) Photoluminescent properties and thermal stability of F-modified aluminosilicate phosphor for solid-state lighting. J Mater Sci Mater Electron 27:906–912
49. Kaky KM, Lakshminarayana G, Baki SO, Lira A, Caldino U, Meza-Rocha AN, Falcony C, Kityk IV, Taufiq-Yap YH, Halimah MK, Mahdi MA (2017) Structural and optical studies of Er^{3+}-doped alkali/alkaline oxide containing zinc boro-aluminosilicate glasses for 1.5 mu m optical amplifier applications. Opt Mater 69: 401–419
50. Assadi AA, Herrmann A, Tewelde M, Damak K, Maalej R, Russel C (2018) Tb^{3+} as a probe for the molecular structure of mixed barium magnesium alumino silicate glasses. J Lumin 199:384–390
51. Righini GC, Ferrari M (2005) Photoluminescence of rare-earth-doped glasses. Riv Nuovo Cimento 28:1–53
52. Wang X, Hu LL, Meng XG, Li HM, Wang SK (2018) Effect of Al_2O_3 and La_2O_3 on structure and spectroscopic properties of Nd-doped sol-gel silica glasses. J Lumin 204:554–559
53. Wu YT, Qiu KH, Tang QX, Zhang WT, Wang JL (2018) Luminescence enhancement of Al^{3+} co-doped $Ca_3Sr_3(VO_4)_4$: Eu^{3+} red-emitting phosphors for white LEDs. Ceram Int 44: 8190–8195
54. Fanai AL, Khan U, Rai S (2019) Luminescence enhancement of Pr^{3+} doped sol-gel silica glass as a result of Al^{3+} co-doping. J Non-Cryst Solids 503:89–93
55. Jankeviciute A, Kareiva A (2011) Synthesis and characterization of leucite ceramics using sol-gel derived molecular precursors. Mendeleev Commun 21:287–288
56. Sinusaite L, Grigoraviciute-Puroniene I, Popov A, Ishikawa K, Kareiva A, Zarkov A (2019) Controllable synthesis of tricalcium phosphate (TCP) polymorphs by wet precipitation: effect of washing procedure. Ceram Int 45:12423–12428
57. Deliormanli AM, Yildirim M (2016) Sol-gel synthesis of 13-93 bioactive glass powders containing therapeutic agents. J Aust Ceram Soc 52:9–19
58. Shi QS, Kang JF, Qu Y, Liu SQ, Khater GA, Li S, Wang YL, Yue YL (2018) Effect of rare-earth oxides on structure and chemical resistance of calcium aluminophosphate glasses. J Non-Cryst Solids 491:71–78
59. Grigoraviciute-Puroniene ZA, Tsuru K, Ishikawa K, Kareiva A (2019) A novel synthetic approach for the calcium hydroxyapatite from the food products. J Sol-Gel Sci Technol 91:63–71
60. Haque FZ, Nandanwar R, Singh P, Dharavath K, Syed FF (2018) Effect of different acids and solvents on optical properties of SiO_2 nanoparticles prepared by the sol-gel process. Silicon 10:413–419
61. Izadifar M, Koeniger F, Gerdes A, Woell C, Thissen P (2019) Correlation between composition and mechanical properties of calcium silicate hydrates identified by infrared spectroscopy and density functional theory. J Phys Chem C 123:10868–10873
62. Ahmadi Z, Moztarzadeh F (2018) Synthesizing and characterizing of gelatin-chitosan-bioactive glass (58s) scaffolds for bone tissue engineering. Silicon 10:1393–1402
63. Wiglusz RJ, Grzyb T, Lis S, Strek W (2009) Preparation and spectroscopy characterization of Eu:$MgAl_2O_4$ nanopowder prepared by modified Pechini method. J Nanosci Nanotechnol 9:5803–5810
64. Skaudzius R, Enseling D, Skapas M, Selskis A, Pomjakushina E, Juestel T, Kareiva A, Ruegg C (2016) Europium-enabled luminescent single crystal and bulk YAG and YGG for optical imaging. Opt Mater 60:467–473
65. Skruodiene M, Katelnikovas A, Vasylechko L, Skaudzius R (2019) Tb^{3+} to Cr^{3+} energy transfer in a co-doped $Y_3Al_5O_{12}$ host. J Lumin 208:327–333
66. Smalenskaite S, Salak AN, Ferreira MGS, Skaudzius R, Kareiva A (2018) Sol-gel synthesis and characterization of hybrid inorganic-organic Tb(III)-terephthalate containing layered double hydroxides. Opt Mater 80:186–196
67. Rozman N, Tobaldi DM, Cvelbar U, Puliyalil H, Labrincha JA, Legat A, Skapin AS (2019) Hydrothermal synthesis of rare-earth modified titania: influence on phase composition, optical properties, and photocatalytic activity. Materials 12:713
68. Ahmed HAAS, Ntwaeaborwa OM, Kroon RE (2013) High efficiency energy transfer in Ce,Tb co-doped silica prepared by sol-gel method. J Lumin 135:15–19
69. Shen YQ, Qiu KH, Wang JL, Zhang WT, Tang QX (2017) Synthesis of Dy^{3+} co-doped $Bi_4Si_3O_{12}$:Sm^{3+} phosphors with enhanced red-emitting properties. Ceram Int 43:15946–15951
70. Pavasaryte L, Katelnikovas A, Klimavicius V, Balevicius V, Momot A, Van Bael MK, Hardy A, Kareiva A (2018) Eu^{3+} − doped $Y_{3-x}Sm_xAl_5O_{12}$ garnet: synthesis and structural investigation. New J Chem 42:2278–2287